D. Lieberman and J. E. Shepherd "Detonation interaction with a Diffuse Interface and Subsequent Chemical Reaction" Shock Waves 16(6):421-430, 2007. Preprint, see journal for final version http://dx.doi.org/10.1007/s00193-007-0080-3

D.H. Lieberman · J.E. Shepherd

Detonation Interaction with a Diffuse Interface and Subsequent Chemical Reaction

Received: date / Accepted: date

Abstract We have investigated the interaction of a detonation with an interface separating a combustible from an oxidizing mixture. The ethylene-oxygen combustible mixture had a fuel-rich composition to promote secondary combustion with the oxidizer in the turbulent mixing zone that resulted from the interaction. Diffuse interfaces were created by the formation of a gravity current using a sliding valve that initially separated the test gas and combustible mixture. Opening the valve allowed a gravity current to develop before the detonation was initiated. By varying the delay between opening the valve and initiating the detonation it was possible to achieve a wide range of interface conditions. The interface orientation and thickness with respect to the detonation wave have a profound effect on the outcome of the interaction. Diffuse interfaces result in curved detonation waves with a transmitted shock and following turbulent mixing zone. The impulse was measured to quantify the degree of secondary combustion, which accounted for 1-5% of the total impulse. A model was developed that estimated the volume expansion of a fluid element due to combustion in the turbulent mixing zone and predicted the resulting impulse increment.

Keywords Detonation · diffuse interface · secondary combustion

D.H. Lieberman

Graduate Aeronautical Laboratories, California Institute of Technology, Pasadena, CA USA

Tel.: +626-437-3192

Fax: +310-754-2799

E-mail: dlieberman@exponent.com *Present address: Exponent Failure Analysis Associates, Los Angeles, CA USA*

J.E. Shepherd

Graduate Aeronautical Laboratories, California Institute of Technology, Pasadena, CA USA E-mail: joseph.e.shepherd@caltech.edu

1 Introduction

When a detonation wave propagating in a gaseous combustible mixture reaches a concentration boundary, a complex interaction results between the detonation and interface between the two gases. The details of this interaction are dependent

on the mixture compositions, the relative geometry of the detonation and interface, and the characteristic thickness of the interface.

In the present study, the interface is a composition gradient between the combustible and non-combustible mixtures. The thickness of the interface is determined by mixing caused by fluid mechanical stirring and diffusion. We classified the extent of the mixing at the interface by comparing the cell size of the detonation with the interface thickness. A sharp interface occurs when the detonation cell size is much greater than the interface thickness.[1] A diffuse interface, the case of the present study, occurs when the detonation cell width in the combustible gas is much less than the interface thickness.

The geometry of a detonation propagating in a composition gradient can be divided into two main categories. The first is when the detonation velocity is parallel to the direction of the gradient, and the second is when it is perpendicular. In general, the composition gradient vector and the detonation velocity vector are not parallel or perpendicular but at some intermediate angle. The first case has been studied by numerous researchers investigating the transmission and successful re-initiation of a detonation across a gap of non-combustible gas ([3], [8], [15], [16]). Other work [7] has examined detonation transmission to an inert gas or other combustible mixture and subsequent reflection off of a rigid end-wall. The current study will focus to a large extent on the perpendicular or nearly-perpendicular case.

When the detonation propagation direction is perpendicular to the mixture gradient, a curved detonation wave results that ultimately decouples into a shock wave and turbulent mixing zone (TMZ), shown in Fig. 1b. This is due in part to the dependence of the detonation velocity on the equivalence ratio. For a detonation modeled as an ideal one-dimensional discontinuity with no affect of curvature on reaction zone structure, the normal component of the curved wave will correspond to the local Chapman-Jouguet detonation velocity. There has been little work done on detonation propagation perpendicular to a continuous composition gradient. Experiments [10] were carried out that measured concentration gradients made by diffusion and used soot foils to characterize the detonation propagation. Other work [4] examined concentration gradients in a numerical study to investigate the possibility of a flame occurring in the incomplete combustion products. Oblique detonations were observed [5] in sharp interface experiments where various combustible mixtures were separated in parallel channels. It is possible for combustion to occur in the turbulent mixing zone (TMZ) by choosing a combustible mixture such that the combustion products are incompletely oxidized. This allows further reactions to take place if the mixture downstream of the interface contains an oxidizer [14]. The aim of the following discussion is to address the key physical issues that arise when a detonation propagates in the direction normal to a concentration gradient. Some of the main issues to be discussed are

[1] We have studied this case and the results will be presented in a companion paper.

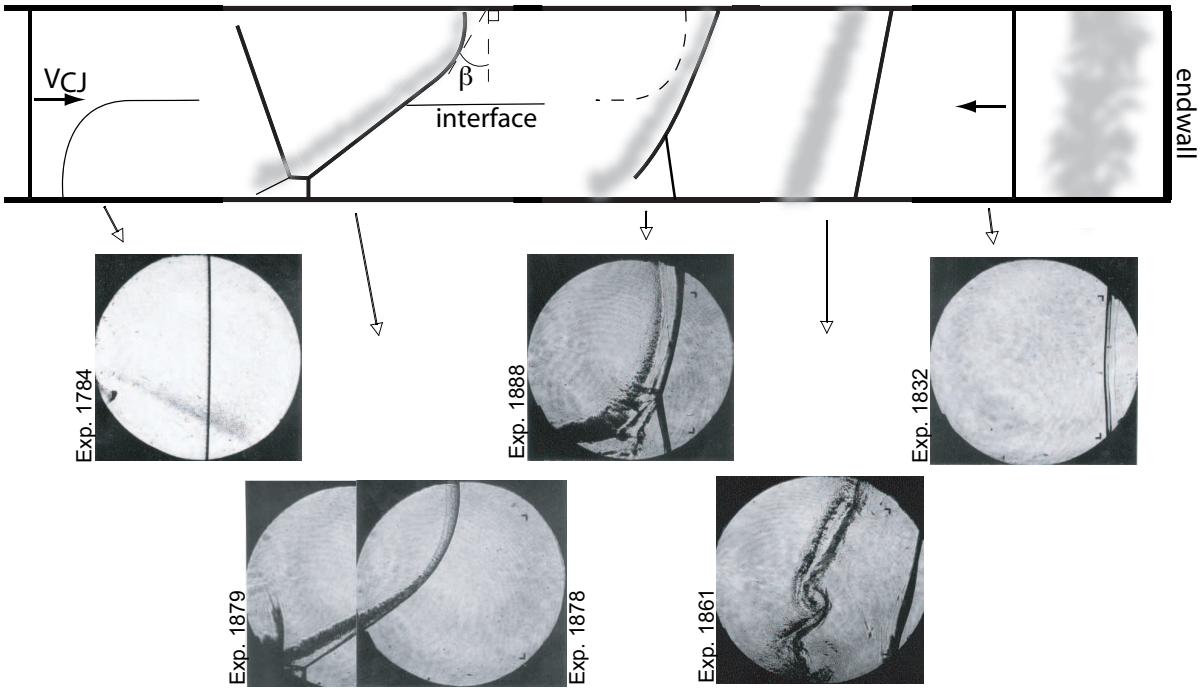

Fig. 1 The interaction of a detonation with a diffuse interface is illustrated with supporting observations from experimental images. A detonation wave (a) interacts with the diffuse interface and forms a curved wave (b). Upon exiting the combustible mixture, the detonation decouples completely resulting in a transmitted shock and TMZ (c) and (d). When the shock reaches the endwall it reflects (e) and interacts for a second time with the interface.

the general shape of the detonation wave, and the decoupling of the shock wave and reaction zone. The presence of secondary combustion between the partially oxidized detonation products and oxidizer in the TMZ is also examined.

2 Experimental setup

The experiments were carried out using the GALCIT Detonation Tube (GDT) [1,2], which is 7.3 m long with an inside diameter of 0.280 m. It is connected to a 0.762 m long square test section with inside dimensions of 0.15 m by 0.15 m. A wave cutting device extends 1 m into the end of the GDT to cut out a square section of the circular detonation front before entering the test section. A sliding valve assembly separates the ethylene-oxygen combustible mixture in the GDT from the oxidizer or inert diluent in the test section during the experimental preparation.

Figure 2 is a view of the test section illustrating the location of the end flange of the GDT, the sliding valve assembly, and the test section. Visualization for the experiments, using a schlieren system [1], was made through an optical viewport (BK7 or quartz windows) that could be arranged in two separate positions. The first position is located 0.275 m downstream of the sliding valve and is referred to as port 1. The second viewport position is located 0.56 m downstream of the sliding valve (see Fig. 2) and is referred to as

port 2. The locations of the pressure transducers and a quartz window on the end wall used for fluorescence imaging are also shown. Fuel rich ethylene-oxygen mixtures occupied the GDT, and either oxygen, nitrogen, or nitrous oxide occupied the test section. The ethylene-oxygen equivalence ratio $\Phi = 2, 2.5, 3$. The initial pressure and temperature for all experiments were 15 kPa and 298 K, respectively. Detonations

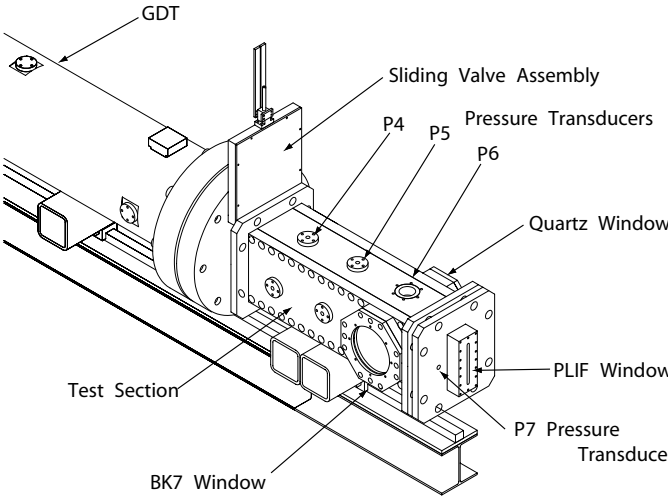

Fig. 2 A schematic of the test section with the sliding valve assembly and the end flange of the GDT.

were initiated in the GDT by discharging a 2 μF bank of capacitors charged to 9 kV through a 0.16 mm copper wire. Detonation velocities were measured to within 5% of the Chapman-Jouguet speed. The cell sizes of the detonations were measured using the soot foil technique [19] and were in all cases below 5 mm.

The diffuse interface was made with a gravity current (GC). The formation and propagation of the gravity current was examined in the test section using acetone planar laser induced fluorescence (PLIF) [12, 17], and in a half-scale water channel [20] to understand the early time development of the GC, see Fig 3. The thickness of the diffuse interface, δ_c, was estimated from the thickness of the region of vorticity obtained from digital particle image velocimetry (DPIV) [9, 20] measurements from the water channel experiments and then re-scaled for the gas phase experiments. In the PLIF experiments, the combustible mixture in the GDT was replaced with an acetone-helium mixture of matched density.

The sliding valve, actuated by a falling mass, was designed to completely isolate both the combustible mixture and test gas, as well as to open sufficiently fast to control the formation of the gravity current. The sliding valve was measured to open in 170 ms with an uncertainty of 10 ms. The mass needed to achieve this opening time was 55 kg.

3 Results and discussion

The general description of this problem, shown as a schematic in Fig. 1, is of a detonation wave propagating through a diffuse interface. The diffuse interface is composed of ethylene-oxygen with $\Phi = 2.5$ above a layer of pure oxygen. The two layer situation was created by allowing a long time to elapse between the creation of the gravity current and detonation initiation (see discussion below). The sequence begins with a detonation wave (a) prior to encountering the diffuse interface. A curved detonation wave (b) results during the interaction leading to a decoupled transmitted shock and TMZ. As the detonation exits the gravity current, what remains is a transmitted shock followed by the TMZ (c). The

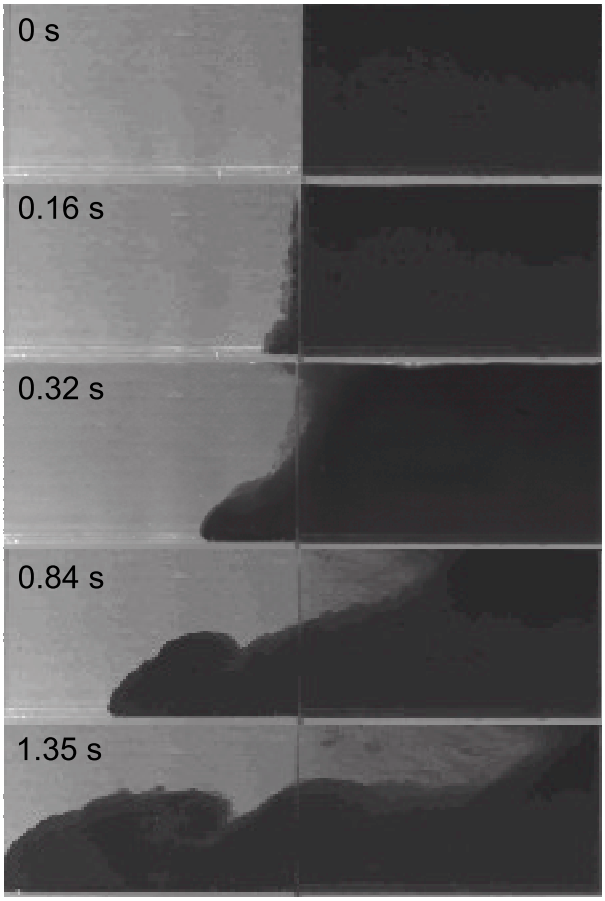

Fig. 3 Time sequence illustrating the development of a gravity current using dye visualization. The gravity current head in the dense fluid (at bottom of image) is propagating from right to left. The dark colored fluid is the salt water solution and the clear fluid is de-ionized water. The plate is completely withdrawn at 0.16 s.

shock wave and TMZ occupy a smaller axial distance than the curved detonation wave with the distance between the shock and TMZ (d) increasing with time. When the shock reaches the endwall it reflects (e) and interacts with the interface a second time. The reflected-shock-interface interaction is not visible as it occurs in the space between the window and the endwall. The complex interaction of the shock wave with the lower experimental boundary Fig. 1b,c produces a Mach reflection.

Gravity currents of various sizes were formed by varying the delay time, defined from the time the sliding valve reaches the open position to the time when a detonation is initiated in the GDT. The range of behavior is shown in Fig. 4 where four separate experiments are shown at different stages of the gravity current development. In these experiments the $\phi = 2.5$ ethylene-oxygen combustible mixture is colored yellow for visibility and flows below the less dense nitrogen gas. Figure 4a is an image of a shock wave followed by a TMZ. The delay time was 0 s, corresponding to a planar interface, and consequently explains why there is no gravity current visible on the overlay. This translates to a leading shock wave that is for the most part perpendicular to the top and bottom surface along with a reflected trailing shock that is possibly due to slight imperfections in the interface shape. As the gravity current grows, the wave structure becomes more curved. Figure 4b shows the transmitted shock, TMZ, and the location of the gravity current before the combustible mixture was detonated with a delay time of 1 s. The leading shock wave is curved with a Mach stem at the top wall. Figure 4c shows the location of the gravity current after a 2 s delay time and the presence of a detonation propagating within 10% of the CJ velocity and transverse waves visible just behind the detonation front at the bottom of the figure. At a 3 s delay time, the curved detonation (Fig. 4d) looks similar to the detonation in Fig. 4c except that the gravity current occupies half the height of the test section thus changing the curvature of the leading wave.

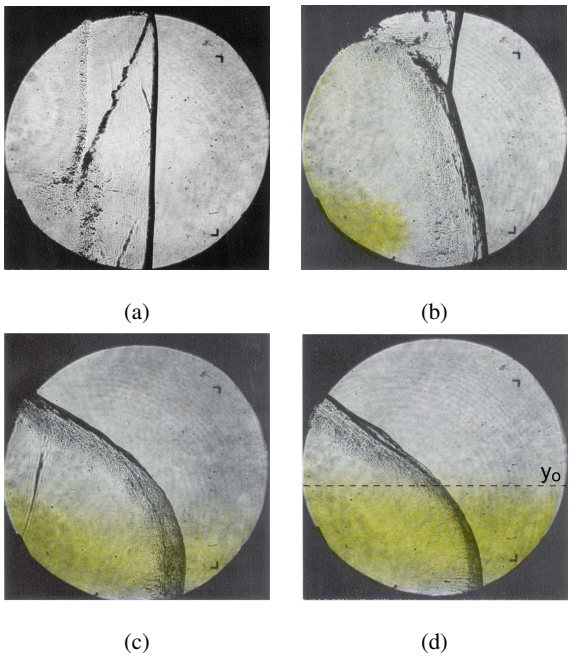

Fig. 4 Four schlieren images from four separate experiments overlaid with the location of the gravity current at the instant of detonation initiation. Ethylene-oxygen (Φ=2.5) is the combustible mixture with pure nitrogen as the test gas. The delay times are 0 s (a), 1 s (b), 2 s (c), and 3 s (d). The vertical height y_o is used to estimate the composition profile.

3.1 Composition gradient

An analysis of the curved detonation wave is made in the special case when the gravity current has a predominantly horizontal orientation as shown in Fig. 4d. In this configuration, experiments indicate the gravity current heads are out of the field of view and the unsteady motion is minimized.

The composition gradient is largely responsible for the curvature and decoupling of the detonation wave due to the Arrhenius dependence of the reaction rates on post-shock temperature and the variation of CJ wave speed with composition. The composition gradient is estimated from the gravity current measurements [12,20] which were carried out specifically to determine the role that the composition profile plays. This analysis considers a horizontal interface as shown in Fig. 4d.

A simple error function profile of the form

$$X_i = \mathscr{C}_1 \left[1 + \mathrm{erf}\left(\frac{y - y_\circ}{\delta_c} \right) \right] + \mathscr{C}_3 \tag{1}$$

is assumed for the species mole fraction X_i as a function of the vertical distance y. The constants $\mathscr{C}_1$, $\mathscr{C}_3$, δ_c, and $y_\circ$ are specific to each experiment and delay time. The error function profile is motivated by appealing to the solution of the diffusion equation as well as knowing the boundary conditions at both limits of the vertical coordinate y. The estimated profiles are only expected to be qualitative since the composition is not known precisely. Turbulent flow structures such as those observed at the interface in Fig. 3 can enhance mixing and result in more complex mixture gradients. Two composition profiles are investigated in this sec-

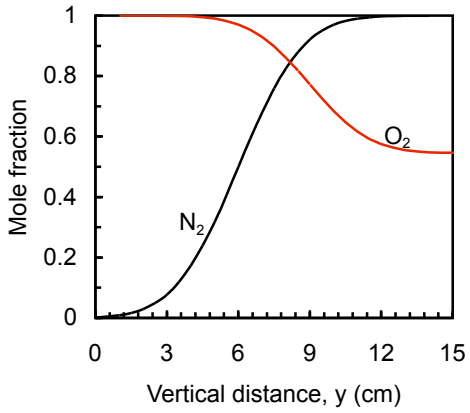

Fig. 5 Estimated mole fraction plotted as a function of vertical distance y in the test section. Two profiles are shown based on Equation (1) for the oxygen dilution case (O_2) and the nitrogen dilution case (N_2).

tion. The first is for a $\Phi = 2.5$ ethylene-oxygen mixture diluted with nitrogen, and the second is for a $\Phi = 2.5$ ethylene-oxygen mixture diluted with oxygen. Diluting with oxygen decreases the equivalence ratio whereas diluting with nitrogen does not alter the equivalence ratio but decreases the volume fraction of combustible mixture. The combustible mixture is located below the nitrogen in the nitrogen dilution case and above the oxygen in the oxygen dilution case since the ethylene-oxygen mixture has a molecular weight of 30 g/mol, which is between that of oxygen and nitrogen. The estimated mole fraction profiles are shown in Fig. 5 as a function of vertical distance in the test section. For oxygen dilution, the mole fraction of oxygen is equal to one at $y = 0$ cm and increases to 0.55 at $y = 15$ cm. For nitrogen dilution the mole fraction of nitrogen is equal to zero at $y = 0$ cm and one at $y = 15$ cm. The constants $\mathscr{C}_1$ and $\mathscr{C}_3$ are determined using the bounding mole fraction values. The constant δ_c is a measure of the diffuse interface thickness and is obtained by measuring the average vorticity thickness in the water channel experiments, shown in Fig. 6 using an edge detection program. It is evident that the vorticity thickness of the interface is not uniform and exhibits a sinuous shape as a result of the turbulent flow structure present at the interface. The average value used in this study is a simplification made for the diffusion based composition gradient model. A complete description of the composition gradient at the interface would need to incorporate these features. The water channel experiments were carried out at half scale using a water and saline solution with matched density differences [12]. The

Table 1 Table of constants used in Equation (1) to specify the composition profile.

composition	$y_\circ$ [cm]	δ_c [cm]	$\mathscr{C}_1$	$\mathscr{C}_3$
O_2	9	3	0.23	0.55
N_2	6	3	0.5	0

values of the constants are listed in Table 1. No effort was made to adjust the constant to fit the wave shape. The ZND

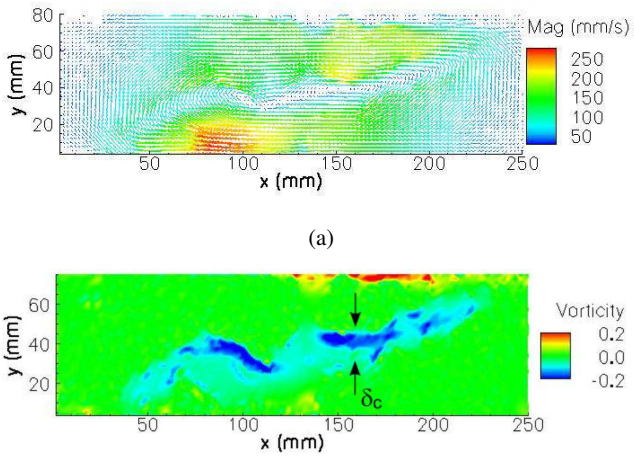

Fig. 6 Velocity (a) and vorticity (b) profiles of a gravity current formed between a saline solution and water with the head propagating to the left. The interface thickness δ_c can be estimated since the density ratio of the liquid phase experiment was chosen to match the gas phase experiments in the GDT.

induction time is plotted as a function of the vertical distance y in Fig. 7. The induction time spans over four orders of magnitude, from microseconds in the undiluted sections of both oxygen and nitrogen profiles, and rapidly rises to milliseconds as the dilution increases. The dramatic increase in induction time has been observed [11] to result in decoupling of the reaction zone from the detonation in the case

of detonation propagation parallel to the gradient direction. The points of decoupling, based on experimental observations are shown. The detonation velocity, determined using

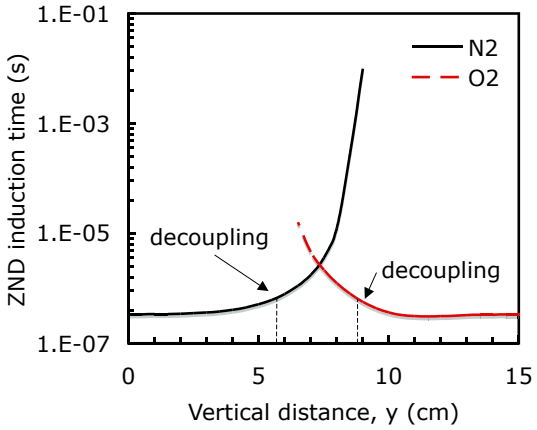

Fig. 7 ZND induction time plotted as a function of vertical distance y in the test section. The profiles are shown for the oxygen dilution case (O_2) and the nitrogen dilution case (N_2).

the composition gradient and the analysis of the detonation shape are compared, and plotted as a function of vertical distance y in Fig. 8. Dilution with nitrogen, at a distance of 0 cm indicates that the detonation velocity equals 2620 m/s, corresponding to the undiluted limit. As the vertical distance increases, the nitrogen dilution increases, resulting in lower detonation velocities. The same is true when diluting with oxygen; however, the decrease in detonation velocity results when decreasing the equivalence ratio. In this case, it turns out that the maximum detonation velocity is at an equivalence ratio of 2.5. In general, instead of the curve decreasing monotonically, there would be a peak at the equivalence ratio corresponding to the maximum detonation velocity.

The detonation shape velocities are obtained from the images using

$$V_{CJ} = V_{CJmax}\cos(\beta) \tag{2}$$

and considering the detonation to have zero thickness. The wave angle β (see Fig. 1) is determined numerically from the wave shape. The maximum detonation velocity is $V_{CJmax} =$ 2620 m/s for an ethylene-oxygen combustible mixture with $\Phi = 2.5$. There is modest agreement between both methods when the vertical distance is small, $y < 2$ cm (or $y > 13$ cm for oxygen mixture compositions). This corresponds to the portion of the curved detonation close to the top wall (Exp. #1878) and bottom wall (Exp. #1884). The spatial pro-

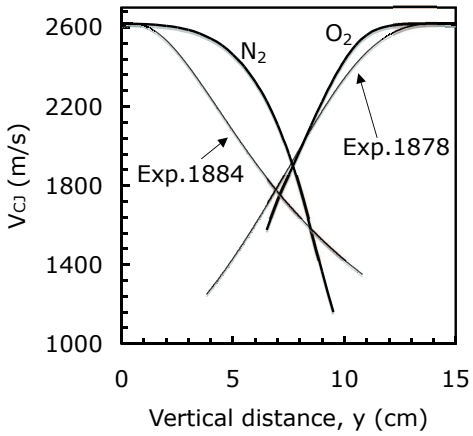

Fig. 8 Detonation velocity plotted as a function of vertical distance (y) in the test section. The profiles are shown for the oxygen dilution case (O_2) and the nitrogen dilution case (N_2).

files of the curved detonation waves from the schlieren images and based on composition profiles based on Equation 1 are determined and compared in Fig. 9. The vertical and axial distances are plotted on the same scale. For both oxygen and nitrogen composition gradients, a good agreement is ob-

served with the experiments below a vertical distance $y = 5$ cm (or $y = 10$ cm for oxygen mixture compositions). The approximate locations of decoupling shown in Fig. 9 are also labeled on the induction time plot (Fig. 7) to give an indication of the mixture sensitivity. The decoupling locations are based on the experimental observations and determined from visual inspection of the images. For both oxygen and nitrogen cases, the decoupling is identified as occurring when the induction time begins to dramatically increase with increasing dilution. It must be emphasized that the results presented in Figures 5 through 9 apply to the limiting case of a long delay time in which case the interface is horizontal.

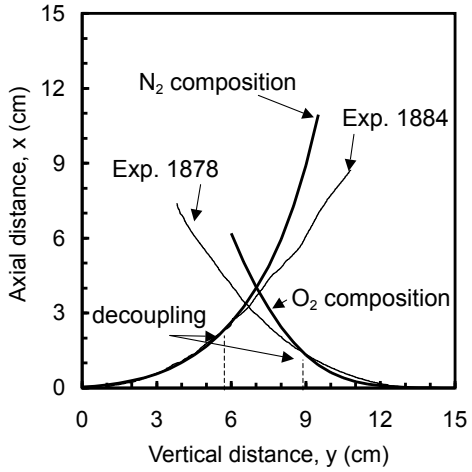

Fig. 9 Estimated wave shape $y(x)$ for the oxygen dilution and the nitrogen dilution cases compared with the experimental results.

3.2 Experimental impulse: the role of secondary combustion

The impulse is calculated from experimental pressure traces to quantify the amount of secondary burning that occurs in the TMZ. This is accomplished by integrating the pressure time histories of the four pressure transducers located in the test section as shown in Fig. 10. The integration is carried out using the two-point Newton-Cotes method and the results reported in MPa· s. The integration of the pressure trace starts at the arrival of the incident shock wave and terminates upon the arrival of pressure disturbances from the GDT approximately 5 ms later. The impulse has an abrupt change in slope at the arrival of the incident and reflected shocks. It was found that with all factors being equal, the impulse was 1-5% higher with oxygen versus nitrogen as the test gas.

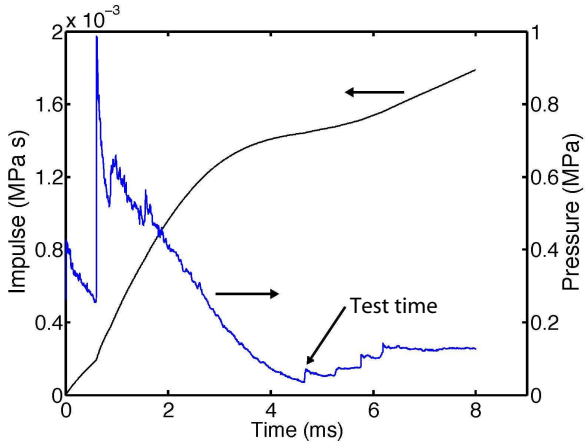

Fig. 10 An overlay of pressure and impulse vs. time at pressure transducer P5. The mixture is composed of $2.5C_2H_4 + 3O_2$ with O_2 as the test gas.

3.2.1 Time scale of combustion

This section addresses the chemical reaction time scale of the partially oxidized combustion products (CO and H_2) and the test gas. The goal is to determine the time-scales required for the reaction to take place and estimate the volume expan-

sion and temperature rise that result. The analysis is carried out by first mixing the detonation products with the shocked test section gas (test gas) keeping the composition frozen and then allowing the reaction to take place at constant pressure and enthalpy [12]. The initial temperature before the reaction takes place is a weighted average of the detonation products and shocked test gas temperatures and determined during the frozen composition mixing.

The results of this model are shown in Fig. 11. The mixture induction time is plotted against the oxygen mass fraction, f_{O_2}, of the composite mixture defined as

$$f_{O_2} = \frac{m_{O_2}}{m_{O_2} + m_{CJ}} \tag{3}$$

where m_{O_2} and m_{CJ} are the masses of oxygen and partially oxidized detonation products, respectively. The induction time in this plot was obtained by finding the time when the temperature time derivative reached 90% of its peak value. The stoichiometric point for this mixture corresponds to f_{O_2}= 0.615. The main result of Fig. 11 is that the induction times for the majority of the oxygen mass fraction range are on the order of a few microseconds. The large induction time values occur in the limit as $f_{O_2} \to 0$ where the partially oxidized detonation products are already in equilibrium and as $f_{O_2} \to 1$ where the temperature of the frozen mixture decreases toward the post-shock temperature of oxygen ($\approx$1600 K). Both the change in temperature and specific volume normalized by the frozen composition state are shown. Both curves peak between $f_{O_2} = 0.8$ and 0.9 because of the decrease of the initial temperature and specific volume as the oxygen mass fraction increases. The values of ΔT and Δv are obtained by taking the difference of the peak value obtained during the reaction and the frozen composition value.

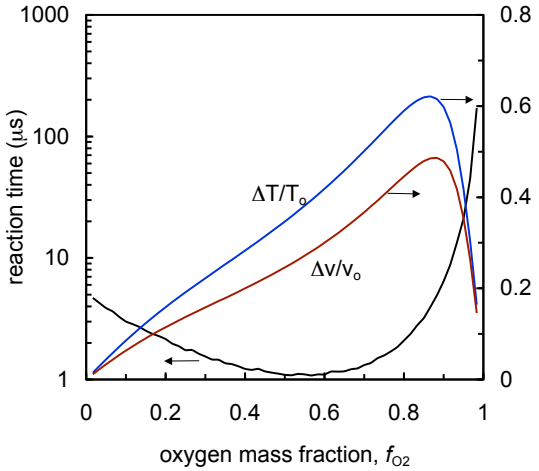

Fig. 11 Induction time vs. oxygen mass fraction computed using a homogeneous mixing ignition time calculation (HMIT) on the left axis. Temperature and specific volume ratio vs. oxygen mass fraction on the right axis

3.3 Secondary impulse model

A simple model is developed to predict the increase in impulse observed in experiments where oxygen is used as a test gas compared to nitrogen. The model estimates the growth of a reacting fluid element in the TMZ given the appropriate time scales, length scales, and degree of mixing. The expansion of the reacted fluid elements produce compression waves that increase the pressure in the flow behind the shock wave and therefore increase the impulse. The secondary impulse model does not account for many of the complex details associated with turbulent shear layers and detonation-composition-gradient interactions that are important in this problem. The goal is to simply verify that the magnitude of

the impulse increment, observed in the experimental pressure histories, is correct.

3.3.1 Model outline

Consider a fluid element, moving in a flow with a convective velocity u_p. The growth of a fluid element resulting from chemical reactions is depicted in Fig. 12. The velocity of the left (δu_p^-) and right (δu_p^+) edges of the fluid element are combined to obtain an expression for the growth rate of the fluid element

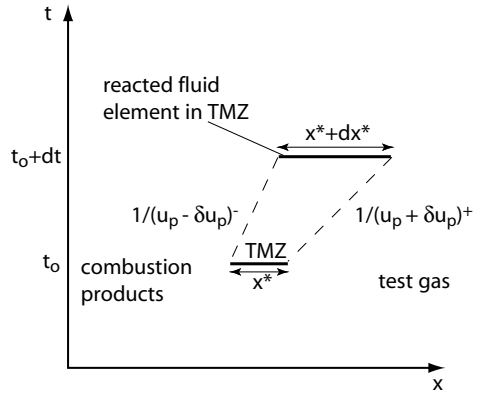

Fig. 12 A sketch of a fluid element expanding during chemical reaction at constant pressure and enthalpy.

$$\frac{dx^*}{dt} = \delta u_p^+ - \delta u_p^-. \tag{4}$$

The increase in pressure is related to the velocity increase using the acoustic equation [13]

$$\delta P = \pm \rho c \, \delta u_p \tag{5}$$

where ρ and c are the local density and sound speed. The use of Equation 5 is motivated by the small increase in pressure observed in experiments with secondary combustion. Substituting Equation 5 into Equation 4 using the plus and minus sign for δu_p^+ and δu_p^- respectively, then isolating for δP results in

$$\delta P = \frac{\overline{\rho c}}{2} \frac{dx^*}{dt}. \tag{6}$$

With the average acoustic impedance $\overline{\rho c}$ defined as

$$\overline{\rho c} = 2 \left(\frac{1}{(\rho c)^+} + \frac{1}{(\rho c)^-} \right)^{-1}, \tag{7}$$

where $(\rho c)^-$ and $(\rho c)^+$ represents fluid to the left and right of the TMZ, namely the combustion products and the test gas, respectively. It is assumed that the thermodynamic states of the test gas and combustion products do not change measurably as a result of chemical reactions in the TMZ. The acoustic analogy is based on the assumption that the chemical reactions occur at constant pressure and enthalpy, appropriate for diffusively controlled combustion within the shear layer.

The impulse I is defined as

$$I = \int P dt \tag{8}$$

where P is the local pressure. The impulse can be decomposed into two parts that represent the bulk flow impulse $I_\circ$ and the increment due to secondary chemical reactions I'. Similarly the pressure is decomposed in the same manner resulting in

$$I = I_\circ + I' = \int P dt = \int (P + \delta P) dt. \tag{9}$$

Isolating the contributions of impulse due to chemical reactions in Equation 9 and substituting Equation 6 for the pressure increment yields after integration

$$I' = \int \delta P dt = \frac{\overline{\rho c}}{2} \Delta x^*. \tag{10}$$

Δx^* refers to the total growth of the fluid element due to chemical reactions and is related to the volume expansion Δv via the expression

$$\frac{\Delta x^*}{x^*} = \frac{\Delta v}{v_\circ}. \tag{11}$$

Substituting Equation 11 into Equation 10 results in

$$I' = \mathscr{C} x^* \frac{\overline{\rho c}}{2} \frac{\Delta v}{v_\circ}. \tag{12}$$

An estimate of I' is obtained by substituting the local unreacted density and sound speed, the experimentally measured value of x^*, and the quantity $\Delta v/v_\circ$, obtained from Sec. 3.2.1. The present computation is clearly only an order of magnitude argument and a constant of proportionality $\mathscr{C}$ has been introduced in Equation 12. The value of $\mathscr{C}$ has to be determined by comparison with the experimental data.

The value x^* in Equation 12 reflects the size of the TMZ visible in port 2 and monotonically increases with delay time. x^* can be increased to account for additional combustion in the TMZ after the shock wave reflects off the end-wall. It has been shown [18] that TMZ growth can increase by a factor of six after the re-shock event. However, in the following calculations all the factors that can amount to an increase in impulse are lumped into the constant $\mathscr{C}$.

The visible growth rate of the shear layer does not increase with the addition of heat release, in fact the growth was shown to decrease [6]. However, the shear layer displacement thickness changes from being negative to positive causing the surrounding fluid to be displaced and generating compression waves.

3.4 Model predictions

Values for the variables on the right hand side of Equation 12 are estimated based on the previous discussion. The thermodynamic variables are specified for f_{O_2}= 0.615 corresponding to a stoichiometric mixture composition. The constant of proportionality $\mathscr{C}$ is varied from a value of 1 to 10 to account for interface growth after the shock reflection off the end-wall. A reference impulse of 1000 kg·m^{-1}·s^{-1} obtained from impulse measurements at pressure transducer P4 is used to calculate the increment.

The model prediction and experimental results for impulse increment are plotted in Fig. 13 as a function of delay time. The experimental impulse increment increases with delay time for pressure transducers P4, P5, and P6 and is bounded between about 1-5%. The model prediction also increases with delay, largely a result of the TMZ thickness dependence on delay time. When the constant $\mathscr{C} = 1$, the model predicts lower impulses than the experiments. Increasing the constant $\mathscr{C}$ to 5 or 10 yields better quantitative agreement. This could be attributed to the importance of further reaction and growth in x^* during the re-shock phase.

Given the simplicity of the model, only order of magnitude agreement can be expected at best. The fact that theory estimates impulses on the same order as the experimental findings indicates that secondary combustion in the TMZ is a plausible explanation for the impulse increment.

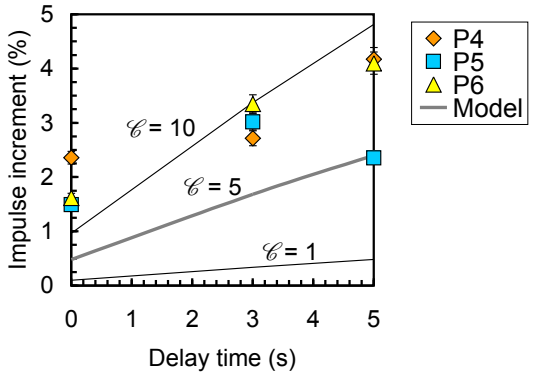

Fig. 13 Impulse increment (%) for oxygen compared to nitrogen versus delay time. The impulse model prediction is plotted for a range of proportionality factors.

4 Conclusion

We have experimentally studied detonation propagation along diffuse interfaces. We have observed the refraction of the detonation wave through the interface and subsequent creation of a turbulent mixing zone from the remains of the interfacial region. By using a fuel-rich ethylene-oxygen combustible mixture and an oxidizing test gas, we were able to observe and quantify the effects of combustion inside the turbulent mixing zone.

The main consequence of the mixture composition gradient through the diffuse interface was to cause the detonation wave to curve: eventually the reaction zone decouples from the leading shock wave when the combustible mixture becomes sufficiently dilute. We attribute the wave curvature to the decrease in lead shock velocity with increasing dilution. The reaction zone behind the curved shock lengthens as the post-shock induction time increases with decreasing shock velocity. The rapid increase in induction time with decrease in shock velocity results in the decoupling of the reaction zone from the shock and the formation of a gap between the transmitted shock and the turbulent mixing zone.

Secondary combustion in the turbulent shear layer was investigated. The measured impulse over a fixed time interval was used as a figure of merit to quantify the degree to which chemical reactions took place. Comparison was made between otherwise identical experiments with the sole difference being the choice of test gas. The impulse difference was between 1-5% in reasonable agreement with the simple impulse model based on the volume expansion of a fluid element in the TMZ.

Acknowledgements Funding for this project was provided by Sandia National Laboratories.

References

1. Akbar, R.: Mach reflection of gaseous detonations. Ph.D. thesis, California Institute of Technology, Pasadena, California (1997)
2. Austin, J.: The role of instability in gaseous detonation. Ph.D. thesis, California Institute of Technology, Pasadena, California (2003)
3. Bull, D., Elsworth, J., McLeod, M.: Initiation of unconfined gas detonations in hydrocarbon-air mixtures by a sympathetic mechanism. In: Proc. of the 7th Int. Coll. on the Dynamics of Explosions and Reactive Systems (ICDERS). GottingenGöttingen, Germany (1979)
4. Calhoon, W., Sinha, N.: Detonation wave propagation in concentration gradients (2005). 43rd AIAA Aerospace Sciences Meeting and Exhibit, Jan. 10-13, 2005 AIAA-2005-1167

5. Dabora, E., Desbores, D., Guerraud, C., Wagner, H.: Oblique detonations at hypersonic velocities. Progg. Aero. Astro. **133**, 187–204 (1991)
6. Dimotakis, P.: Turbulent Free Shear Layer Mixing and Combustion, *Prog. Astro. Aero.*, vol. 137, chap. 5, pp. 265–340. American Institute of Aeronautics and Astronautics, Inc. (1991)
7. Donato, M., Donato, L., Lee, J.: Transmission of detonations through composition gradients. In: Proceedings of the First Specialists Meeting of The Combustion Institute. Bordeaux, France (1981)
8. Engebretsen, T., Bjerketvedt, D., Sonju, O.: Propagation of Gaseous Detonations Through Regions of Low Reactivity, *Prog. Astro. Aero.*, vol. 153, pp. 324–346. American Institute of Aeronautics and Astronautics, Inc. (1991)
9. Huang, H., Dabiri, D., Gharib, M.: On errors of digital particle image velocimetry. Meas. Sci. Technol. **8**, 1427–1440 (1997)
10. Ishii, K., Kojima, M.: Propagation of detonations in mixtures with concentration gradients. In: G. Roy, S. Frolov, J. Shepherd (eds.) Application of detonation to propulsion (2004)
11. Kuznetsov, M., Dorofeev, S., Efimenko, A., Alekseev, V., Breitung, W.: Experimental and numerical studies on transmission of gaseous detonation to a less sensitive mixture. Shock Waves **7**, 297–304 (1997)
12. Lieberman, D.: Detonation interaction with sharp and diffuse interfaces. Ph.D. thesis, California Institute of Technology, Pasadena, California (2005)
13. Liepmann, H., Roshko, A.: Elements of Gasdynamics. Dover (2001)
14. Pintgen, F., Shepherd, J.: Secondary pressure waves from rich fireballs. In: 20th International Colloquium on the Dynamics of Explosions and Reactive Systems. ICDERS, Montreal, Canada (2005)
15. Teodorczyk, A., Benoan, F.: Interaction of detonation with inert gas zone. Shock Waves **6**, 211–223 (1996)
16. Thomas, G., Sutton, P., Edwards, D.: The behaviour of detonation-waves at concentration gradients. Combustion and Flame **84**(3-4), 312–322 (1991)
17. Thurber, M., Hanson, R.: Pressure and composition dependences of acetone laser-induced fluorescence with excitation at 248, 266, and 308 nm. Appl. Phys. B **69**, 229–240 (1999)
18. Vetter, M., Sturtevant, B.: Experiments on the richtmyer-meshkov instability of an air/sf6 interface. Shock Waves **4**(5), 247–252 (1995)
19. White, D.: Turbulent structure of gaseous detonations. The Physics of Fluids **4/4**, 465–480 (1961)
20. Wolf, M., Lieberman, D., Shepherd, J.: Characterization of gravity currents in a water channel for use in detonation refraction experiments. FM2005-006, Graduate Aeronautical Laboratories, California Institute of Technology (2005)